Synthesis of Cerium-Activated Yttrium Aluminate Based Fine Phosphors by an Aerosol Route

Lidija Mancic,[a] Vesna Lojpur,[a] Ignacio Barosso,[b] Maria Eugenia Rabanal,[b] and Olivera Milosevic*[a]

[a] Institute of Technical Sciences of SASA, Knez Mihailova 35/IV, 11000 Belgrade, Serbia
∗ Fax: +38-1112185263 E-mail: olivera.milosevic@itn.sanu.ac.rs

[b] Department of Materials Science and Engineering and Chemical Engineering, University Carlos III of Madrid, Avd. Universidad 30, 28911 Leganes, Madrid, Spain

Abstract: Polycrystalline fine powders of yttrium aluminate doped with Ce^{3+} were synthesised by spray pyrolysis of a polymeric pre-cursor, which was obtained by dissolving the corresponding nitrates in a solution of ethylenediaminetetraacetic acid (EDTA) in ethylene glycol (EG). Aerosol decomposition was performed at 550 °C followed by an additional thermal treat-ment (900–1100 °C). The yield of either a single yttrium alu-minium perovskite (YAP) phase or a single yttrium alumin-ium garnet (YAG) phase was investigated as a function of the predefined yttrium/aluminium ratio, the cerium doping concentration, the processing temperature, and the thermal-treatment regime, which included the variation of the heat-ing and cooling rates (dT/dt), the residence time (τ), and the atmosphere. Changes in the composition and structure of the precursor during thermal decomposition were investigated by thermogravimetric and differential thermal analysis (TGA/DTA) and FTIR spectroscopy. The particle morphology and structure were analysed by a combination of scanning electron microscopy and energy-dispersive X-ray spec-troscopy (SEM/EDS) and by high-resolution transmission electron microscopy (HR-TEM). The structural refinement was based on the phase identification performed by X-ray powder diffraction (XRPD). The emission spectra were re-corded within the range 325–800 nm by applying excitation wavelengths of 297 (YAP) and 450 nm (YAG). The employed synthesis conditions assured the formation of spherical, non-agglomerated particles with well-developed surfaces and diameters between 200 and 800 nm. For a predefined Y/Al ratio of 1:1, lower processing temperatures combined with longer heat treatments under stationary conditions resulted in a multiphase system, composed of YAP, YAG, and mono-clinic yttrium aluminate (YAM) phases. However, a short heat treatment with a high heating rate (200 °C/min) at higher temperatures results in the formation of a kinetically favoured pure YAP hexagonal phase. On the other hand, for a predefined Y/Al ratio of 3:5, the generation of a thermody-namically favoured pure YAG phase has been confirmed, re-gardless of the applied heat-treatment conditions. Although incomplete, Ce^{3+} introduction into the host matrix has been detected by XRPD and luminescence measurements.

Keywords: Yttrium aluminates / Nanoparticles / Luminescence / Polymerization / Spray pyrolysis

Introduction

Cerium(III)-activated yttrium aluminates have under-gone extensive research for different display applications in electronics and optoelectronics because of their efficient lu-minescence properties and their good thermal, mechanical, and chemical stability.[1–3] As for system phases, Ce(III)-doped yttrium aluminium garnet (YAG:Ce^{3+}), is a suitable material for the nonpolluting production of white light with high energy efficiency.[2] Moreover, yttrium aluminium per-ovskite (YAP) is a suitable host phosphor material for mi-crowave and high-frequency applications because of its low dielectric constant.[3] In addition, both cerium-doped YAP and YAG are promising fast scintillators for synchrotron X-ray experiments and they are suitable for applications related to medical imaging, such as positron emission tomography (PET), single-photon emission tomography (SPET), gamma-ray cameras, and so on.[4–7]

These systems have been described in the literature in three different kinds of crystal phases:[8,9] yttrium alumin-ium perovskites, yttrium aluminium garnets, and mono-clinic yttrium aluminate (YAM) with yttrium/aluminium ratios as presented in Table 1. Yttrium aluminium perov-skite has three kinetically favoured forms: hexagonal, or-thorhombic, and cubic. Literature records suggest that

Table 1. Crystal phases in a Y_2O_3–Al_2O_3 system.

Crystal phase, formula	Y/Al	Crystal structure and symmetry
Perovskite, YAP: $YAlO_3$	1:1	cubic orthorhombic, *Pnma* (or *Pbnm*) hexagonal (P_63cm)
Garnet, YAG: $Y_3Al_5O_{12}$	3:5 (or 0.6:1)	cubic, *Ia*–3*d*
YAM:$Y_4Al_2O_9$	(2:1)	monoclinic orthorhombic

many materials exhibit a distorted orthorhombic *Pnma* structure and a hexagonal $P_6 3cm$ form as well; the latter practically loses its similarity to the perovskite symmetry because of a high distortion level. This phase has been found exclusively in chemically synthesised powders.[9,10] The YAPs represent the metastable forms of the yttria–alumina system, and they are commonly formed together with stable YAG and YAM phases as a result of the dissociation reaction described by Equation (1).

$$7YAlO_3 \leftrightarrow Y_4Al_2O_9 + Y_3Al_5O_{12} \quad (1)$$

The crystal structure of cubic garnet, $Y_3Al_5O_{12}$, which has space group *Ia*–3*d*, can be explained as a disordered, closely packed array of oxygen atoms of isometric symmetry, forming AlO_6 octahedra and AlO_4 tetrahedra, with Y^{3+} ions in a O_8 dodecahedron.[11] The Y^{3+} ions can be partially substituted by rare earth ions.

Pure-phase synthesis in yttria–alumina systems is very hard to achieve, even through soft-chemistry routes, and it still presents a challenge since the formation of other phases occurs simultaneously. The yttria–alumina phase diagram,[12,13] in which the ratio of 2:1 refers to the formation of monoclinic $Y_4Al_2O_9$ and 3:5 refers to the formation of garnet $Y_3Al_5O_{12}$, evidences that the structures of the compositions are not straightforward and that the equilibrium reaction [Equation (1)] leads rather to dissociation than to the formation of the multiphase system.

In comparison to conventional solid-state processing, in which high temperatures and long residence times are necessary, current phosphor materials are usually produced through soft-chemistry routes, which have many advantages with regard to the structural and morphological features of the phosphors. Anticipating that nanostructuring will enable a prosperous future development of optical devices, characterised by high brightness, reliability, low power consumption, and a long life of phosphor materials, various efficient wet-chemical synthesis routes have been developed, including sol–gel,[14] combustion processing,[15,16] co-precipitation methods,[17] hydrothermal synthesis,[18,19] and so on.

An aerosol route such as spray pyrolysis (SP) is an effective, direct method intended to provide nanostructured particles with spherical morphology, no agglomerates, good crystallinity and a uniform distribution of luminescent centres in the host material, properties that consequently contribute to the improvement of optical characteristics of materials.[20,21] SP involves extreme synthesis conditions occurring at the level of a micrometer-sized aerosol droplet in a disperse system, thus enabling the synthesis of metastable structures, as previously reported.[21,22] There are certain process parameters, such as high heating and cooling rates, short residence times, and an additional thermal treatment, which may affect the yield of either thermodynamically (YAG, YAM) or kinetically (YAP) stable phases.[12] The introduction of organic components into the solution is becoming increasingly popular, since these components provide the retention of the proper stoichiometry during the process, and the reaction that occurs in the solution leads to volume precipitation and the formation of dense particles. A pure YAP phase can already be synthesised through a classical sol–gel route, but the obtained particles are of irregular shape and size, which is due to extensive agglomeration.[23–27]

In our previous work, we presented the synthesis of pure YAG:Ce^{3+} particles with spherical shape and filled morphology from a polymeric precursor solution containing ethylenediaminetetraacetic acid (EDTA), ethylene glycol (EG), and the corresponding nitrates.[28] Continuing our previous research, in this paper we study the controlled aerosol synthesis of pure phosphor particles consisting of yttria–alumina as a function of processing parameters and the regime of an additional thermal treatment, which includes the variation of the heating and cooling rates (dT/dt), the residence time (τ), and the atmosphere.

Results and Discussion

The Polymer Precursor

Differential thermal and thermogravimetric analyses (DTA/TGA) were performed in order to determine the decomposition mechanism of the polymeric precursor (Figure 1). The first dehydration-related weight loss (ca. 12 wt.-%) occurs at temperatures up to 200 °C, followed by a more striking, sharper change (weight loss of ca. 32 wt.-%) in the TG curve, which is associated with CO_2 and NO_x release. Several peaks between 290 and 505 °C indicate bond breaking in the organic and nitrate compounds. According to the literature, pure EDTA decomposes endothermically at temperatures between 220 and 280 °C in one step, while the ignition of its derivatives (exothermic) is initiated at approximately 500 °C. Pure ethylene glycol would show a strong endothermic peak at 200 °C as a result of boiling.[29] As already pointed out, the decomposition of common yttrium and aluminium nitrate precursors is an endothermic process occurring in several steps at temperatures between 150 and 400 °C, with the most intense peaks at 200 °C and

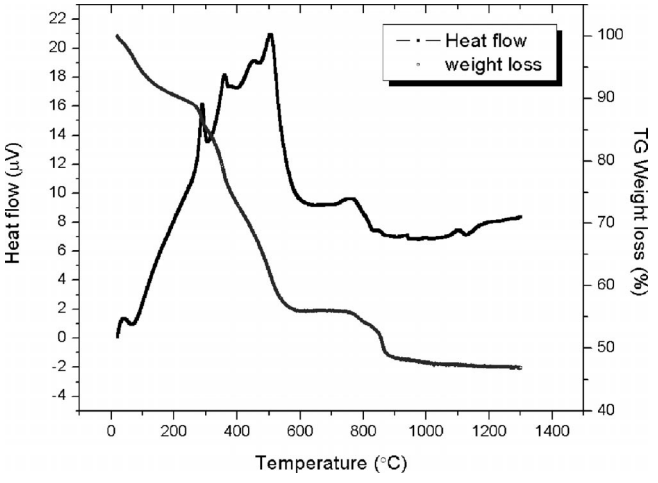

Figure 1. DTA and TGA curves for the polymeric YAP precursor.

390 °C.[30] Figure 1 leads to the conclusion that in this case these steps overlap with the decomposition of the organic phase, which results in a massive formation of gases (weight loss of ca. 44 wt.-%) that stops at approximately 600 °C. A final loss of volatile compounds from the polymeric precursor is registered at 760 and 850 °C (ca. 8 wt.-%). The crystallization of the YAP phase is indicated by a small peak at 1100 °C.[31]

The changes in the composition and structure of the precursor that occurred upon heating were followed by FTIR spectroscopy. Figure 2 shows FTIR spectra of YAG precursors dried at 150 °C with and without the addition of organic components as well as spectra of charred (250 °C) and calcined (1100 °C) polymeric precursor. The intense and wide band with a peak at 3360 cm^{-1} in the spectrum of the pure nitrate precursor (Figure 2a) originates from OH^- stretching vibrations, and its intensity decreases with the addition of EDTA and EG (Figure 2b), which points to the formation of hydrogen bonds.[32] The vibrations of NO_3^- in the polymeric precursor result in the appearance of several peaks between 800 and 1400 cm^{-1} (Figure 2b),[33] while the characteristic N–O stretching vibration of the pure nitrate precursor is reflected as a strong absorption at 1482 cm^{-1} (Figure 2a).[34] In both precursors, bending vibrations of H_2O are clearly noticeable at 1632 cm^{-1}. The effect of EDTA on the synthesis process from polymeric precursor is indicated by the appearance of bands that originate from asymmetric (at ca. 1600 cm^{-1}) and symmetric (at ca. 1530 cm^{-1}) stretching vibrations of metal-coordinated COO^- groups. The esterification of EDTA with EG is verified by the appearance of asymmetric stretching modes at 1093 cm^{-1} and 1338 cm^{-1} referring to C–O–C and =C–O–C groups, respectively.[35] These modes become more pronounced with the increasing temperature and are presented in the inset of Figure 2. As confirmed later on by XRD and TEM analyses, cross-linking of chemical bonds in the polymeric precursor resulted in the formation of a pure YAG phase. The powder that was obtained from calcination of the YAG polymeric precursor at 1100 °C showed IR bands of vibrational modes characteristic of the YAG structure only (i.e., Y–O stretching vibrations in tetrahedral arrangements and Al–O stretching vibrations in octahedral arrangements), which appear at 785, 720, 685, 566, 448, and 425 cm^{-1} (Figure 2d).[36] The absorption band of physically adsorbed CO_2 is also visible at 2360 cm^{-1}, while bands characteristic of organic groups completely disappeared.

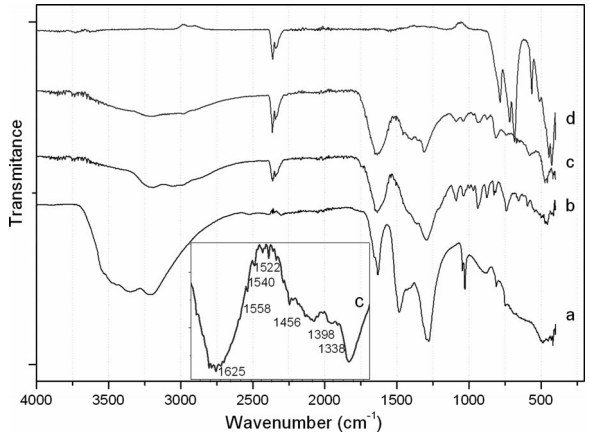

Figure 2. FTIR spectra of (a) pure nitrate precursor dried at 150 °C, (b) polymeric YAG precursor dried at 150 °C, (c) polymeric YAG precursor charred at 250 °C, and (d) YAG powder calcined for 12 h at 1100 °C.

The FTIR results imply the following mechanism for the transition of the polymeric precursor upon heating: first, because of its strong chelating ability, deprotonated H_4EDTA ($C_{10}H_{16}N_2O_8$) binds to metal(III) ions (M^{3+} = Al^{3+}, Y^{3+}) by four oxygen atoms from carboxyl groups and two nitrogen atoms. Since this reaction is faster in the presence of OH^- ions, NH_4OH is usually added to the EDTA solution. Binding as proposed, the hexadentate ligand creates an octahedral structure for aqueous $[M^{III}EDTA]^-$, as presented in Figure 3, which has been confirmed for the solid compound $(NH_4)[Al(EDTA)]\cdot 2H_2O$.[37] However, in $(NH_4)[Y(EDTA)]\cdot 5H_2O$, the structure around M^{3+} changes to a nine-coordinate environment, which is due to the additional bonding of Y^{3+} with the oxygen atoms of three water molecules.[38] With the addition of ethylene glycol, cross-linking should be realized through the formation of the following bonds: carboxyl groups of the $[M^{III}EDTA]^-$ complexes form esters with the hydroxy groups of EG, nitrogen atoms of the complexes also react with the hydroxy groups of EG, and hydrogen bonds are formed between the carbonyl groups of EDTA and the hydroxy groups of EG.[39] Having this in mind, we presume that during the successive SP steps (evaporation, drying, and precipitation) solvent evaporation from the droplets leads to polycondensation of the metal chelates, whereby volume precipitation is promoted, which results in the generation of dense particles.

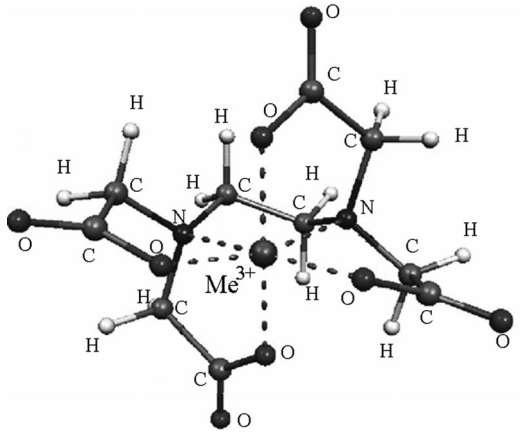

Figure 3. Proposed octahedral structure for aqueous $[M^{III}EDTA]^-$.

The YAP Phase

Phases in a Y–Al–O system doped with 5 at.-% of Ce (regime I) and synthesised with a predefined Y/Al ratio of 1:1 were identified on the basis of the XRPD data presented

in Figure 4. Multicomponent powders were obtained in all cases. The results of Pawley refinements (Table 2) imply that the phase compositions of powders calcined at different temperatures differ significantly. The prevalence of a hexagonal YAP phase (JCPDS 74–1334) is observed for calcination at 900 °C, while its orthorhombic modification (JCPDS 89–7947) is detected for higher temperatures. With rising temperature, the content of the cubic YAG (JCPDS 33–0040) phase increases, while YAM (JCPDS 34–0368) and cubic CeO_2 (JCPDS 81–0792) phases are present as minor fractions in all samples. A hump at $2\theta \approx 30°$ indicates the retention of an amorphous phase in the samples. The formation of cerianite (CeO_2) implies incomplete substitution of yttrium with cerium. However, as it will be shown later, a characteristic green-yellow emission, detected in the photoluminescence spectra, confirmed the introduction of cerium into the garnet structure. The sample treated at 900 °C had a high content of a metastable hexagonal phase, which usually appears in a small amount as an intermediate[9] within a narrow temperature frame during the synthesis of orthorhombic phases. This revealed the possibility of generating this metastable phase in pure form by using this method. In order to get this kinetically favoured phase, a higher heating rate of the droplets and particles during aerosol decomposition at 900 °C was established, while the duration of the additional thermal treatment was reduced to 1 h. The XRPD pattern of a sample synthesised under these conditions is shown in Figure 5. The position of the

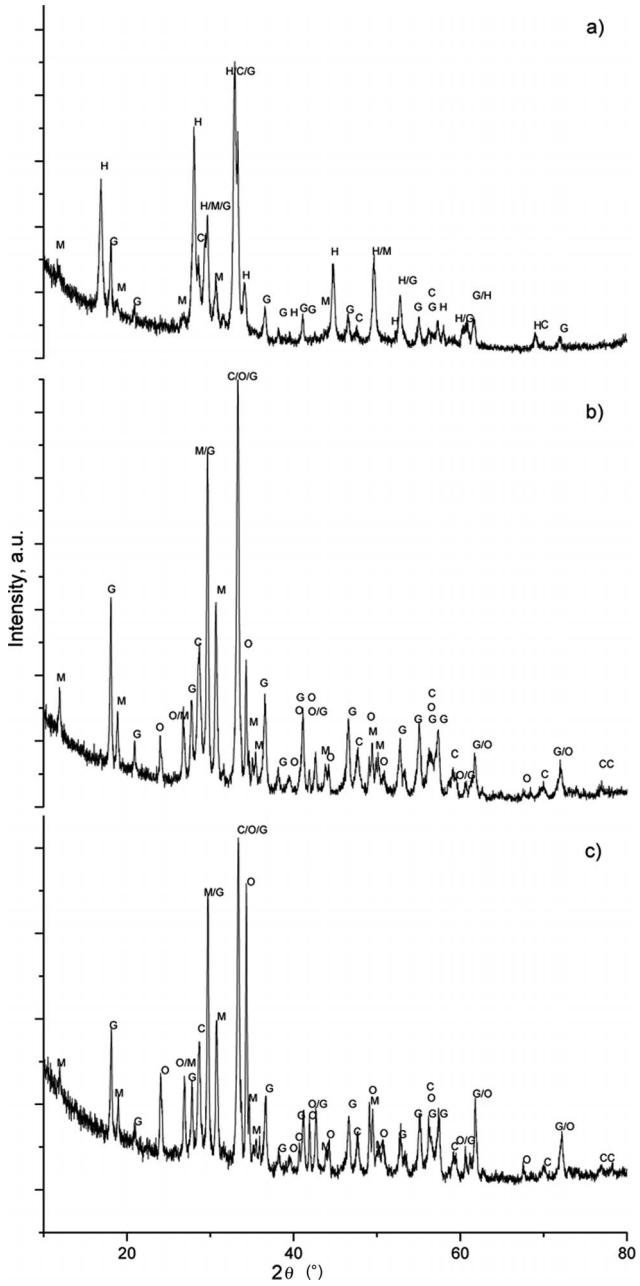

Figure 4. XRPD patterns of Y–Al–O phases synthesised through spray pyrolysis at 550 °C and subsequent treatment at (a) 900 °C, (b) 1000 °C, and (c) 1100 °C for 12 h (regime I). H = YAP hexagonal, O = YAP orthorhombic, G = YAG, M = YAM, C = CeO_2.

Table 2. Microstructural parameters of the phases in a Y–Al–O system, doped with 5 at.-% Ce, synthesised through spray pyrolysis at 550 °C and subsequently treated at elevated temperatures for 12 h (regime I).

	900 °C	1000 °C	1100 °C
YAP hex $P6_3/mmc$	a = 3.673(1) Å c = 10.503(2) Å CS[a] = 35(4) nm		
YAP Orthorhombic $Pbnm$		a = 5.187(1) Å b = 5.326(1) Å c = 7.376(1) Å CS = 269(0) nm strain = 0.09(1) %	a = 5.183(1) Å b = 5.325(1) Å c = 7.374(1) Å CS = 215(1) nm strain = 0.07(1) %
YAG Cubic Ia–$3d$	a = 12.036(1) Å CS = 56(0) nm strain = 0.29(1) %	a = 12.043(1) Å CS = 84(9) strain = 0.27(1) %	a = 12.031(1) Å CS = 84(9) nm strain = 0.22(1) %
YAM Monoclinic $P21/a$	a = 7.349(4) Å b = 10.591(8) Å c = 11.037(7) Å β = 108.25(5) ° CS = 19(7) nm	a = 7.385(1) Å b = 10.452(1) Å c = 11.151(1) Å β = 108.74(1) ° CS = 76(4) nm	a = 7.380(1) Å b = 10.446(2) Å c = 11.132(2) Å β = 108.81(1) ° CS = 73(3) nm
CeO_2 Cubic $Fm\bar{3}m$	a = 5.499(1) Å CS = 18(1) nm	a = 5.402(1) Å CS = 18(9) nm	a = 5.404(1) Å CS = 29(1) nm

[a] CS: crystallite size.

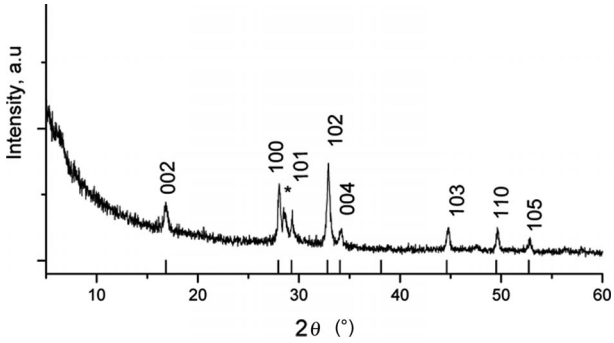

Figure 5. XRPD pattern of pure hexagonal YAP phase synthesised through spray pyrolysis at 900 °C and subsequent treatment at 900 °C for 1 h (regime II). Reflections originating from CeO_2 are indicated with *.

peaks suggests that a hexagonal YAP phase was formed without any other Y–Al–O phases. The lattice parameters obtained through a Pawley refinement are: a = 3.675(1) Å and c = 10.515(4) Å. The presence of CeO_2 in the powder is indicated by the appearance of its strongest reflection (110) at 2θ = 28.54° (marked with * in Figure 5).

Information regarding the morphology and chemical composition of the particles was obtained on the basis of scanning electron microscopy (SEM) and energy-dispersive X-ray spectroscopy (EDS) analyses (Figures 6 and 7). In all cases, highly spherical, loosely agglomerated particles were obtained, the size of which varied from 200 to 800 nm. It is clear that low-temperature processing at 550 °C, followed by a long heat treatment (12 h) at higher temperatures (900–1100 °C) ensures the generation of particles with a high specific surface area (regime I). Nanosized primary subunits, formed through volume precipitation in the droplets during the SP process, generate sponge-like surfaces after subsequent heating of the resulting powder at 900 °C (Figure 6a). With an increase in temperature, the grain-like texture of the particle surface is more pronounced, the porosity is noticeably higher, and sometimes entirely separated primary particles can be recognised in the samples (Figure 6b, c). However, processing at a higher temperature (900 °C) followed by a short heat treatment (1 h) with a high heating rate generates smooth particles, which is due to a lower crystallinity of the YAP phase (regime II), Figure 4.

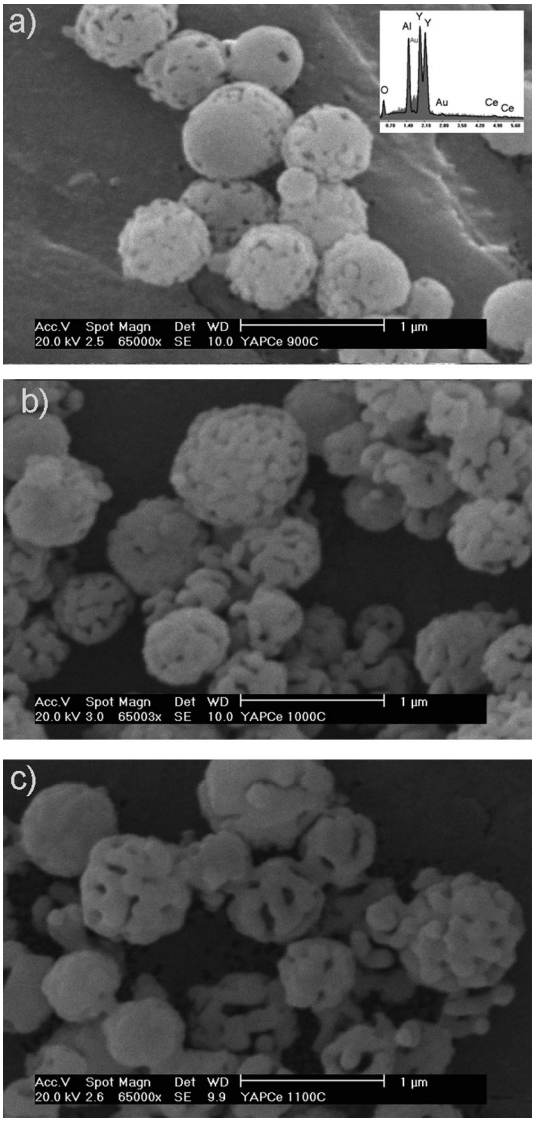

Figure 6. SEM/EDS analyses of particles synthesised from a polymeric precursor solution (Y/Al = 1:1) through spray pyrolysis at 550 °C and subsequent treatment for 12 h (regime I) at (a) 900 °C, (b) 1000 °C, and (c) 1100 °C.

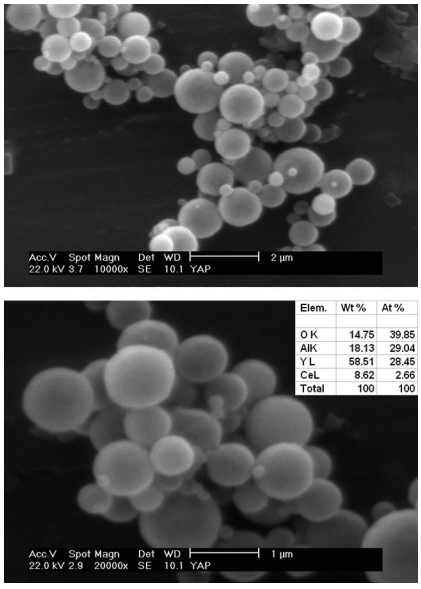

Figure 7. SEM analysis of particles synthesised from a polymeric precursor solution (Y/Al = 1:1) through spray pyrolysis at 900 °C and subsequent treatment at 1100 °C for 1 h (regime II). The inset presents the result of a semiquantitative EDS analysis.

The presence of coarser (size ca. 1 µm) particles indicates a change in the mechanism of particle densification. A higher heating rate decreases the diffusion time during SP and averts further particle shrinkage. Although less visible at the surface, the porosity is sufficient to prevent the particle from bursting as a result of the volatilization of gaseous products formed during precursor decomposition. No residual organic components were detected during chemical analyses. For all samples, EDS confirms the high purity of the particle and the predefined Y^{3+}/Al^{3+} cation ratio of approximately 1:1 (insets in Figures 6 and 7).

The YAG Phase

Figure 8 shows the XRPD pattern of a sample obtained by SP of the polymeric precursor with a predefined Y/Al ratio of 3:5 doped with 2 at.-% of Ce. The precursor was processed at 550 °C and heat-treated at 1100 °C for 12 h (regime I). All diffraction lines can be readily attributed to a pure cubic YAG structure with the space group *Ia*–3*d*. Table 3 presents refined crystal cell parameters together with crystallite sizes and microstrains. All refinement-related data are given in the Supporting Information. An in-

crease of the unit cell parameters and the Y–O bond lengths[40] implies Ce^{3+} incorporation into the garnet lattice. Nevertheless, only partial substitution is established. CeO_2 formation is evident from the detection of its reflections (111) and (220) in the XRPD spectra.

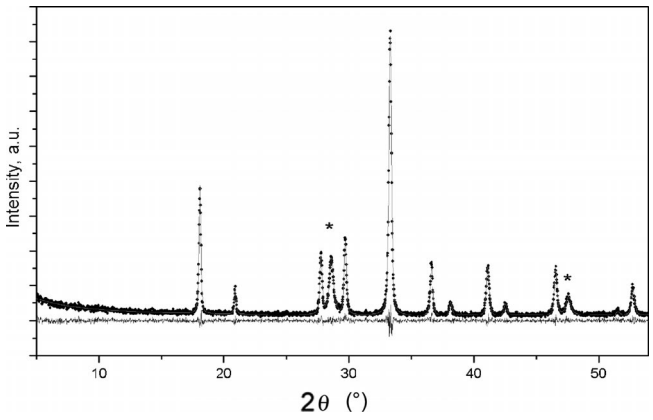

Figure 8. Rietveld refinement of a XRPD pattern of a pure cubic YAG phase synthesised through spray pyrolysis at 550 °C and subsequent treatment at 1100 °C for 12 h (regime I). Reflections originating from CeO_2 are indicated with *.

Table 3. Rietveld refinement details and corresponding reliability factors for a YAG:Ce^{3+} phase synthesised through spray pyrolysis at 550 °C and subsequent treatment at elevated temperatures for 12 h (regime I).

	YAG:Ce^{3+}
Space group	*Ia–3d*
a (Å)	12.0274(6)
Crystallite size (nm)	76(6)
Microstrain (%)	1.131(6)
R_{Bragg} (%)	1.45
Goodness of fit	1.062

The influence of the heat treatment at 1100 °C on the particle morphology is evident from the SEM images presented in Figure 9. Despite the fact that the particles kept their spherical shape to a certain degree, a prolonged heating time leads to their partial decomposition and to stronger agglomeration. In principle, the particles are generated through volume precipitation and contain smaller grains, organized in a spherical shape predefined by the droplet. A closer look at the grains on the particle surface revealed their high crystallinity (Figure 10). The observed interplanar spacing of 0.4251 Å (inset in Figure 10b) correlates well with the *d* value of the (220) plane of the cubic YAG phase (0.4247 Å, JCPDS 33–0040). The continuous expansion of this plane through a whole grain, as seen in Figure 10b, points to the fact that the grains are single crystals.

As already mentioned, among different yttrium aluminate phases both the orthorhombic YAP phase and the cubic YAG phase represent optically active materials when doped with Ce^{3+}, having efficient near-UV emission. This emission originates from parity-allowed electric dipole transitions between excited-state 5d and ground-state 4f orbitals in Ce^{3+}.

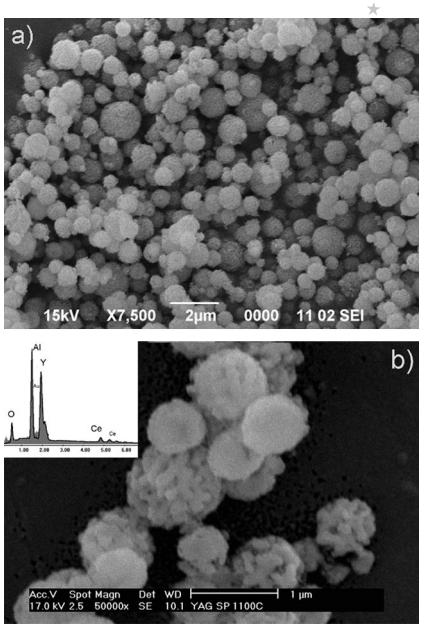

Figure 9. SEM/EDS analyses of particles synthesised from a polymeric precursor solution (Y/Al = 3:5) through spray pyrolysis at 550 °C and subsequent treatment at (a) 1100 °C for 3 h and (b) 12 h (regime I).

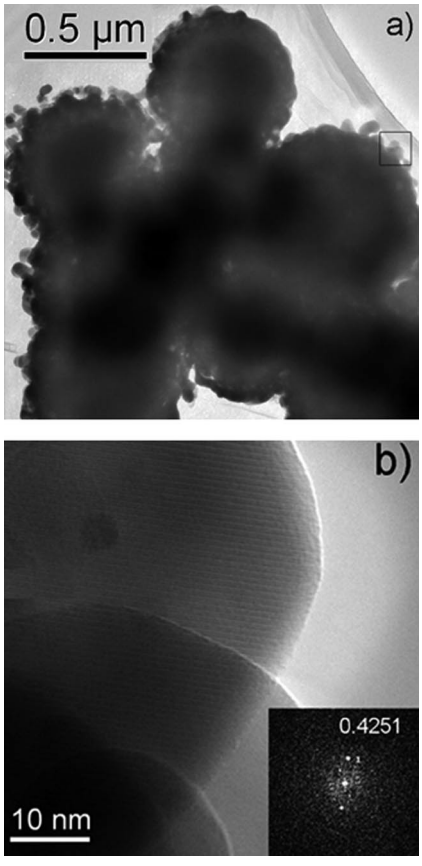

Figure 10. TEM/HR-TEM analyses of particles synthesised from a polymeric precursor solution (Y/Al = 3:5) through spray pyrolysis at 550 °C and subsequent treatment at 1100 °C for 3 h (regime I). The inset shows the fast Fourier transform.

Because of crystal field effects, 5d orbitals have their energy levels divided into at least two sublevels (^2E and $^2T_2$), while the lowest sublevels of 5d can be further split into new components because of spin–orbit interactions. This also applies to the ground-state level 4f, which splits into the components $^2F_{5/2}$ and $^2F_{7/2}$.[6] When the crystal field effect is strong, the splitting of the 5d levels is so large that the Ce^{3+} emission shifts to the visible region. This is the case for the garnet structure, which exhibits a broad emission band in the range 500–650 nm corresponding to a green-yellow luminescence. In contrast, because of its lower crystal field energy, the orthorhombic YAP phase doped with Ce^{3+} emits light at approximately 370 nm.[23] The emission spectra of samples synthesised through spray pyrolysis at 550 °C and subsequent treatment at elevated temperatures for 12 h (regime I), which contain mixtures of orthorhombic YAP and YAG phases, are given in Figure 11. The luminescence peaking at λ = 571 nm proves the incorporation of Ce^{3+} into the garnet phase in all samples. No peaks were observed in the range typical for emissions from YAP:Ce^{3+} (inset in Figure 11), which implies that regardless of the YAP/YAG phase content ratio prolonged powder heating enhances Ce^{3+} incorporation into the cubic crystal structure. The similar luminescence intensity implies a similar level of Ce^{3+} incorporation at the yttrium position in the garnet crystal unit. This can also be deduced from similar values of the crystal unit parameter *a*, given in Table 2. Figure 11d shows the spectrum of a pure YAG phase synthesised through spray pyrolysis at 550 °C and subsequent treatment at 1100 °C. The more narrow and blueshifted emission band peaking at 520 nm can also be ascribed to the transition of an excited electron from the ^2D_j orbital to the $^2F_{5/2}$ and $^2F_{7/2}$ ground states. The observed change in the emission wavelength could be a consequence of lower level of Ce^{3+} incorporation into the garnet lattice,[41] which is confirmed by a smaller change of the lattice parameter (*a* values for YAG in Tables 2 and 3). Hence, a better crystal cell arrangement (confirmed by HR-TEM) results in the narrowing of the emission band in the photoluminescence spectra.

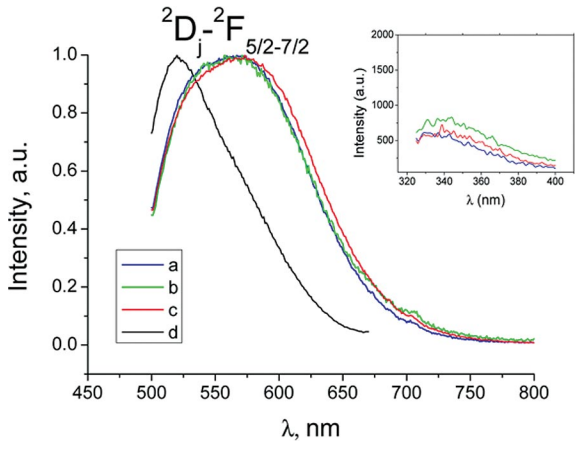

Figure 11. Photoluminescence emission spectra of particles synthesised from a polymeric precursor solution (Y/Al = 1:1) through spray pyrolysis at 550 °C and subsequent treatment for 12 h (regime I) at (a) 900 °C, (b) 1000 °C, and (c) 1100 °C. Photoluminescence emission spectrum (d) of particles synthesised from a polymeric precursor solution (Y/Al = 3:5) through spray pyrolysis at 550 °C and subsequent treatment for 3 h at 1100 °C (regime I).

Conclusions

Highly spherical, non-agglomerated, and dense particles of Ce^{3+}-activated yttrium aluminate phosphors were obtained through spray pyrolysis of polymeric precursor solutions. Although beneficial, the addition of EDTA/EG to the common nitrate precursor is not sufficient for the generation of a pure YAP phase. For predefined cation ratios, lower temperatures during spray pyrolysis combined with longer heat treatments in stationary conditions led to the generation of multiphase systems, while a short processing at higher temperatures combined with a high heating rate (200 °C/min) during calcination resulted in the stabilization of the kinetically favoured hexagonal YAP phase. The generation of the thermodynamically favoured pure YAG phase was confirmed, regardless of the applied heat-treatment conditions.

Experimental Section

Precursor Preparation: Polymeric precursor solutions were prepared from yttrium nitrate [$Y(NO_3)_3{\cdot}6H_2O$, 99.9%, Sigma–Aldrich], aluminium nitrate [$Al(NO_3)_3{\cdot}9H_2O$, 99.9%, Sigma–Aldrich], cerium nitrate [$Ce(NO_3)_3{\cdot}6H_2O$, 99.9%, Sigma–Aldrich], ethylenediaminetetraacetic acid ($C_{10}H_{16}N_2O_8$, EDTA), and ethylene glycol ($C_2H_6O_2$, EG). Yttrium and aluminium nitrates were mixed in molar ratios of 1:1 (for the synthesis of the YAP phase) and 3:5 (for the synthesis of the YAG phase). The ratio of EDTA to the total amount of metal ions was 1:1, while the ratio EDTA/EG was 1:4. The cerium concentration ranged from 2 to 5 at.-%. For the metal-

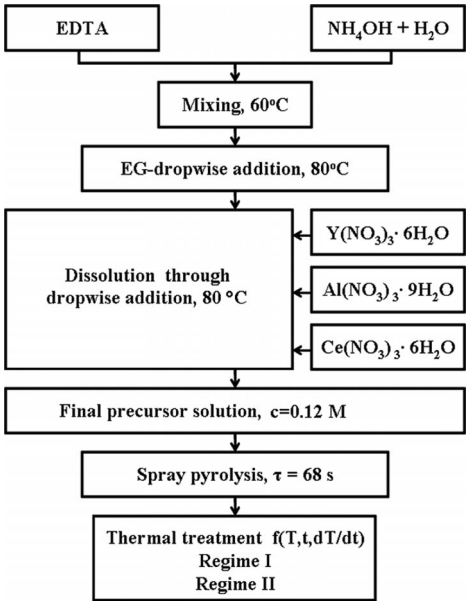

Scheme 1. Procedure for the preparation of polymeric precursor and the subsequent powder processing.

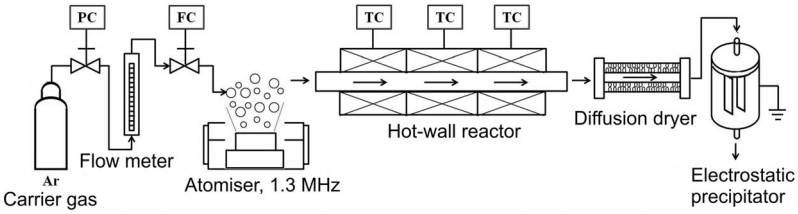

Scheme 2. Experimental setup for spray pyrolysis.

ion complexation and the subsequent esterification, the following procedure was applied: EDTA (0.1 mol) was dissolved in ammonium hydroxide solution at 60 °C and after that slowly added to EG (0.4 mol) while raising the temperature to 80 °C. All nitrates were separately dissolved in demineralised water, and the resulting solutions were added dropwise to the main solution. Ammonium hydroxide was continuously added to prevent EDTA precipitation during nitrate addition. After completion of the addition, the pH value was adjusted to 0.5 with HNO_3. There was no sign of precipitation in the course of the synthesis, but the colour of the solution changed to pale yellow. The procedure for the preparation of the polymeric precursor and the powder processing is given in Scheme 1.

Powder Preparation: The prepared precursor solution was placed in a 1.3 MHz ultrasonic atomiser. From there it was introduced as an aerosol by using Ar as a carrier gas into a hot-wall tubular reactor with three independent heating zones. The droplet–particle residence time (τ) in the reactor was 68 s. In all experiments, the decomposition temperature was set to either 550 or 900 °C for the YAP synthesis and 550 °C for the YAG synthesis. The as-prepared powders were collected in an electrostatic precipitator and additionally treated at 900, 1000, and 1100 °C for either 1, 3, or 12 h in air. Two heating regimes were applied during the thermal treatments to evaluate the phase stabilization and to prevent the composite inhomogeneities: heating in a chamber furnace under stationary conditions (heating and cooling rates of approximately 6 °C/min, regime I) and fast heating in a tubular furnace (heating rate of approximately 200 °C/min, regime II). The experimental setup used for spray pyrolysis is given in Scheme 2.

Characterization: Compositional and structural changes of the precursor during thermal decomposition were investigated by TGA/DTA and FTIR. TGA/DTA measurements were performed with a SETARAM SET-SYS Evolution-1750 instrument at a heating rate of 10 °C/min. FTIR spectra were recorded at room temperature with a Nicolet spectrophotometer (Model 380, Thermo Nicolet Corporation, Madison, USA). The powder phases were identified by XRPD with an X′Pert Philips diffractometer operating with Cu-K_α radiation at 40 mA and 40 kV (data range = 5–100°, scan step: 0.02°, time per step: 10 s). The fundamental parameter approach (FPA) with the Topas Academic 4.1 software[42] was applied for structure refinement. The background was refined by using the sixth-order Chebichev function, while peak profile shapes were convoluted through a Pawley analysis (Lorentzian and Gaussian type for crystallite size and strain components) or a Rietveld analysis (predefined double-Voigt approach for crystallite size). After the convergence, atomic positions and isotropic temperature factors were also included in the refinement. The morphological features and chemical purity of the particles were investigated by scanning electron microscopy (Philips SEM XL30/EDS Dx4) and transmission electron microscopy (JEOL 2010 operating at 200 kV). For the scope of the TEM analyses, the samples were prepared by ultramicrotomy, in compliance with the following procedure: a small quantity of powder was embedded in a resin and then cut to 90 nm thick foils in an ultramicrotome (Reichert–Jung). Steady-state fluorescence was measured with an Edinburgh spectrofluorometer. An optical fibre cable was used for exciting the sample and collecting the fluorescence. In all cases, the excitation and emission slits were set to 5 mm. The excitation wavelengths were 297 (YAP) and 450 nm (YAG). The fluorescence was recorded in the range 325–800 nm.

Supporting Information (see footnote on the first page of this article): Topas[42] outputs and refined microstructural data for the YAG:Ce^{3+} structure.

Acknowledgments

The authors gratefully acknowledge the Ministry of Science and Education of the Republic of Serbia (Project No 172035), the University Carlos III (Madrid, Spain), and the Santander Bank (Chairs of Excellence Program for the academic year 2010–2011) for financial support. The help of Dr. Dragana Jovanovic from the Vinca Institute, Belgrade, with the FTIR analyses is highly appreciated.

[1] C. P. Khattak, F. F. Y. Wang, "Perovskites and Garnets" in *Handbook on the Physics and Chemistry of Rare Earths* (Eds.: K.°A. Gschneidner Jr., L. Eyring), North-Holland Publishing Company, **1979**, vol. 3, pp. 525–607.
[2] K. Zhang, W. Hu, Y. Wu, H. Liu, *Ceram. Int.* **2009**, *35*, 719–723.
[3] B. Basavalingu, H. N. Girish, K. Byrappa, K. Soga, *Mater. Chem. Phys.* **2008**, *112*, 723–725.
[4] S. Mathur, H. Shen, R. Rapalaviciute, A. Kareiva, N. Donia, *J. Mater. Chem.* **2004**, *14*, 3259–3265.
[5] N. Kalivas, I. Valais, D. Nikolopoulos, A. Konstantinidis, A. Gaitanis, D. Cavouras, C. D. Nomicos, G. Panayiotakis, I. Kandarakis, *Appl. Phys. A* **2007**, *89*, 443–449.
[6] T. B. de Queiroz, C. R. Ferrari, D. Ulbrich, R. Doyle, A. S. S. de Camargo, *Opt. Mater.* **2010**, *32*, 1480–1484.
[7] D. Cao, G. Zhao, J. Chen, Q. Dong, Y. Ding, Y. Cheng, *J. Alloys Compd.* **2010**, *489*, 515–518.
[8] J. Marchal, T. John, R. Baranwal, T. Hinklin, R. R. Laine, *Chem. Mater.* **2004**, *16*, 822–831.
[9] K. M. Kinsman, J. McKittrack, *J. Am. Ceram. Soc.* **1994**, *77*, 2866.
[10] S. M. Sim, K. A. Keller, T. I. Mah, *J. Mater. Sci.* **2000**, *35*, 713–717.
[11] A. Beltran, J. Andres, J. A. Igualada, J. Carda, *J. Phys. Chem.* **1995**, *99*, 6493–6501.
[12] M. Nyman, J. Caruso, M. J. Hampden-Smith, T. T. Kodas, *J. Am. Ceram. Soc.* **1997**, *80*, 1231–1238.
[13] C. K. Ullal, K. R. Balasubramaniam, A. S. Gandhi, V. Jayaram, *Acta Mater.* **2001**, *49*, 2691–2699.
[14] P. A. Tanner, P. T. Law, K. L. Wong, L. Fu, *J. Mater. Sci.* **2003**, *38*, 4857–4861.
[15] X. Guodong, Z. Shengming, Z. Junji, X. Jun, *J. Cryst. Growth* **2005**, *279*, 357–362.

[16] S. Ramanathan, M. B. Kakade, S. K. Roy, K. K. Kutty, *Ceram. Int.* **2003**, *29*, 477–484.
[17] J. G. Li, T. Ikegami, J. H. Lee, T. Mori, *J. Am. Ceram. Soc.* **2000**, *83*, 2866–2869.
[18] B. Basavalingu, H. N. Girish, K. Byrappa, K. Soga, *Mater. Chem. Phys.* **2008**, *112*, 723–725.
[19] M. Blosi, S. Albonetti, M. Dondi, A. L. Costa, M. Ardit, G. Cruciani, *J. Sol-Gel Sci. Technol.* **2009**, *50*, 449–455.
[20] O. Milosevic, L. Mancic, M. E. Rabanal, J. M. Torralba, B. Yang, P. Townsend, *J. Electrochem. Soc.* **2005**, *152*, 707–713.
[21] Y. Wang, O. Milosevic, L. Gomez, M. E. Rabanal, J. M. Torralba, B. Yang, P. D. Townsend, *J. Phys. Condens. Matter* **2006**, *18*, 9257–9272.
[22] D. Dosev, B. Guo, M. I. Kennedy, *Aerosol Sci. Technol.* **2006**, *37*, 402–412.
[23] M. Harada, A. Ue, M. Inoue, X. Guo, K. Sakuari, *Scripta Mater.* **2001**, *44*, 2243–2246.
[24] M. Harada, M. Goto, *J. Alloys Compd.* **2006**, *408–412*, 1193–1195.
[25] J. F. Carvalho, F. S. De Vicente, N. Marcellin, P. Odier, A. C. Hernandes, A. Ibanez, *J. Therm. Anal. Calorim.* **2009**, *96*, 891–896.
[26] J. F. Carvalho, F. S. De Vicente, S. Pairis, P. Odier, A. C. Hernandes, A. Ibanez, *J. Eur. Ceram. Soc.* **2009**, *29*, 2511–2515.
[27] S. Wang, Y. Xu, P. Lu, C. Xu, W. Cao, *Mater. Sci. Eng. B* **2006**, *127*, 203–206.
[28] L. Mancic, K. Marinkovic, B. A. Marinkovic, M. Dramicanin, O. Milosevic, *J. Eur. Ceram. Soc.* **2010**, *30*, 577–582.
[29] M. Galceran, M. C. Pujol, M. Aguilo, F. Dıaz, *J. Sol-Gel Sci. Technol.* **2007**, *42*, 79–88.
[30] L. Mancic, G. del Rosario, Z. Marinkovic, O. Milosevic, *Mater. Sci. Forum* **2006**, *518*, 107–112.
[31] J. F. Carvalho, F. S. De Vicente, N. Marcellin, P. Odier, A. C. Hernandes, A. Ibanez, *J. Therm. Anal. Calorim.* **2009**, *96*, 891–896.
[32] J. B. Zhang, P. Y. Zhang, K. Ma, F. Han, G. H. Chen, X. H. Wei, *Sci. China Ser. B* **2008**, *51*, 420–426.
[33] X. H. Li, J. L. Dong, H. S. Xiao, P. D. Lu, Y. A. Hu, Y. H. Zhang, *Sci. China Ser. B* **2008**, *51*, 128–137.
[34] G. Xia, S. Zhou, J. Zhang, J. Xu, *J. Cryst. Growth* **2005**, *279*, 357–362.
[35] M. Motta, C. V. Deimling, M. J. Saeki, P. N. Lisboa-Filho, *J. Sol-Gel Sci. Technol.* **2008**, *46*, 201–207.
[36] A. Lukowiak, R. J. Wiglusz, m. Maczka, P. Gluchowski, W. Strek, *Chem. Phys. Lett.* **2010**, *494*, 279–283.
[37] X. S. Jung, Y. K. Chung, D. M. Shin, S. D. Kim, *Bull. Chem. Soc. Jpn.* **2002**, *75*, 1263–1267.
[38] J. Wang, X. Zhang, Y. Zhang, Z. Liu, *Wuhan Univ. J. Nat. Sci.* **2003**, *8*, 1131–1137.
[39] C. Mao, L. Zhou, X. Wu, X. Sun, *Supercond. Sci. Technol.* **1996**, *9*, 994–1000.
[40] F. Euler, J. A. Bruce, *Acta Crystallogr.* **1965**, *19*, 971–978.
[41] Y. C. Kang, I. W. Lenggoro, S. B. Park, K. K. Okuyama, *Mater. Res. Bull.* **2000**, *35*, 789–798.
[42] A. A. Coelho, *Topas-Academic*, **2006**.